J Optim Theory Appl (2015) 167:733–760
DOI 10.1007/s10957-015-0749-1

Adjoint-Based Optimization on a Network of Discretized Scalar Conservation Laws with Applications to Coordinated Ramp Metering

Jack Reilly[1] · **Samitha Samaranayake**[1] · **Maria Laura Delle Monache**[2] · **Walid Krichene**[1] · **Paola Goatin**[2] · **Alexandre M. Bayen**[1]

Received: 24 October 2013 / Accepted: 4 May 2015 / Published online: 5 October 2015

Abstract The adjoint method provides a computationally efficient means of calculating the gradient for applications in constrained optimization. In this article, we consider a network of scalar conservation laws with general topology, whose behavior is modified by a set of control parameters in order to minimize a given objective function. After discretizing the corresponding partial differential equation models via the Godunov scheme, we detail the computation of the gradient of the discretized system with respect to the control parameters and show that the complexity of its computation scales linearly with the number of discrete state variables for networks of small vertex degree. The method is applied to the problem of coordinated ramp metering on freeway networks. Numerical simulations on the I15 freeway in California demonstrate an improvement in performance and running time compared with existing methods. In the context of model predictive control, the algorithm is shown to be robust to noise in the initial data and boundary conditions.

Keywords Control of discretized PDEs · Network of hyperbolic conservation laws · Adjoint-based optimization · Transportation engineering · Ramp metering

Mathematics Subject Classification 35L65 · 90-08

Communicated by Emilio Frazzoli.

✉ Jack Reilly
jackdreilly@berkeley.edu

[1] University of California, Berkeley, CA, USA

[2] Inria Sophia Antipolis - Méditerranée, Sophia Antipolis, France

1 Introduction

In this paper, we propose a discrete adjoint approach to compute optimal ramp metering strategies on road networks modeled by conservation laws. Networks of one-dimensional conservation laws, described by systems of nonlinear first-order hyperbolic *partial differential equations* (PDEs), are an efficient framework for modeling physical phenomena, such as freeway traffic evolution [1–3] and supply chains [4]. Similarly, PDE systems of balance laws are useful in modeling gas pipeline flow [5,6] and water channels [7,8]. Optimization and control of these networks is an active field of research [9–11]. More generally, numerous techniques exist for the control of conservation laws, such as, for example, backstepping [12,13], Lyapunov-based methods [12], and optimal control methods [14–16].

In particular, a common approach consists in computing the gradient of the cost functional via the *adjoint method* [17–19]. Nevertheless, its implementation in the framework of nonlinear conservation laws presents several difficulties linked to the discontinuous character of the solutions. In particular, the presence of shocks in the solutions requires a careful sensitivity analysis based on the use of shift differentials and generalized tangent vectors; see [20–22]. Extensive study exists also on the choice of method for effectively computing the gradient via the adjoint. In particular, the continuous adjoint method [9,23–25] operates directly on the PDE and a so-called adjoint PDE system, which, when solved, can be used to obtain an explicit expression of the gradient of the underlying optimization problem. Conversely, the discrete adjoint method [9,11,17] first discretizes a continuous-time PDE and then requires the solution of a set of linear equations to solve for the gradient. Finally, a third approach exists, which uses automatic differentiation techniques to generate an adjoint solver from the numerical representation of the forward system [26,27].

It is well known that the numerical treatment of the adjoint method imposes a careful choice of the discretization scheme to avoid the introduction of numerical errors at discontinuities [28]. Rigorous convergence results for optimization problems have been provided for Lax–Friedichs-type schemes [29] and relaxation methods [30]. The case of road networks in free-flow conditions is addressed in [9]. In our more general setting of PDE networks and applications to freeway traffic control, the presence of junction conditions, with both forward and backward-moving shockwaves, led us to use a modified Godunov scheme, which precisely takes into account the flows at the network nodes. An alternative approach involves using Lax–Friedichs-type discretizations with higher-resolution interpolation schemes [31]. Moreover, general existence and stability results for the corresponding system of equations modeling traffic evolution on the network are still missing at the moment. Therefore, establishing rigorous convergence results for the gradient computation in this framework is out of the scope of this paper. Here, we made the choice of the discrete adjoint approach, which derives the gradient directly from the discretized system, thus avoiding dealing with weak boundary conditions in the continuous system [1,2,32].

There exist many applications of the adjoint method for control, optimization and estimation of physical systems in engineering. Shape optimization of aircraft [24,25,33] has applied the method effectively to reduce the computational cost in gradient methods associated with the large number of optimization parameters. The

technique has also been applied in parameter identification of biological systems [19]. State estimation problems can be phrased as optimal control problems by setting the unknown state variables as control parameters and penalizing errors in resulting state predictions from known values. This approach has been applied to such problems as open water state estimation [34] and freeway traffic state estimation [35].

Since conservation laws may be nonlinear by nature and lead to nonconvex or nonlinear formulations of the corresponding optimization problem, fewer efficient optimization techniques exist for the discretized version of these problems than for convex problems, as one example. One approach is to approximate the system with a "relaxed" version in order to use efficient linear programming techniques. In transportation, by relaxing the Godunov discretization scheme, the linearization approach was used in [36] for optimal ramp metering and in [37] for optimal route assignment, having a zero relaxation gap under certain modeling assumptions. The ramp metering technique in [38] uses an additional control parameter (variable speed limits) to mimic linearized freeway dynamics. While the upside of these methods is reduced computational complexity and the guarantee of finding a globally optimal solution, the downside is that the model of the linearized physical system may greatly differ from the actual system to which the control policies would be applied.

Another approach avoids discretization of the continuous system by taking advantage of certain simplifying assumptions in the dynamics. In [39], the problem of finding optimal split ratios on a traffic network is efficiently solved by deriving nonlinear and linear algebraic formulations of a simplified form of the continuous system dynamics which only considers forward-moving shockwaves. In [40], a mixed-integer linear program (MILP) formulation is posed for the optimal routing of goods on a supply chain, leading to efficient solutions of this particular application. The number of integer constraints needed in the MILP formulation is proportional to the number of nonlinear constraints in the underlying system and has a direct impact on the efficiency of MILP solvers.

Applications to highly nonlinear systems such as freeway traffic may prefer nonlinear programming approaches such as the adjoint method using nonlinear discretization techniques, which avoid integer constraints and allow the constraints to capture more complex dynamics. This approach leads to more expensive optimization algorithms, such as gradient descent, and does not guarantee finding a global optimum. One difficulty in this approach comes in the computation of the gradient, which, if using finite differences, requires a full forward simulation for each perturbation of a control parameter. This approach is taken in [41] to compute several types of decentralized ramp metering strategies. The increased complexity of the finite differences approach for each additional control parameter makes the method unsuitable for real-time application on moderately sized freeway networks.

Ramp metering is a common freeway control strategy, providing a means of dynamically controlling freeway throughput without directly impeding mainline flow or implementing complex tolling systems. While metering strategies have been developed using microscopic models [42], most strategies are based off macroscopic state parameters, such as vehicle density and the density's relation to speed [43–45]. Reactive metering strategies [46–48] use feedback from freeway loop detectors to target a desired mainline density, while predictive metering strategies [11,36,41,49] use a

physical model with predicted boundary flow data to generate policies over a finite time horizon. Predictive methods are often embedded within a model predictive control loop to handle uncertainties in the boundary data and cumulative model errors [38].

The rest of the article is organized as follows. Section 2 gives an overview of scalar conservation law networks and their discretization via the Godunov method, while introducing the nonlinear, finite-horizon optimal control problem. Section 3 details the adjoint method derivation for this class of problems and shows how it can be used to compute the gradient in time and memory space linear in the number of discrete state and control variables. Section 4 applies the adjoint method to the problem of optimal coordinated ramp metering. Numerical results on a model of a 19.4-mile freeway network in California are given in Sect. 5. Section 6 gives open questions and future work.

2 Preliminaries

2.1 Conservation Law PDEs

In this paper, we focus on scalar hyperbolic conservation laws. In particular, we consider the nonlinear transport equation of the form:

$$\partial_t \rho\,(t,x) + \partial_x f\,(\rho\,(t,x)) = 0 \quad (t,x) \in \mathbb{R}_+ \times \mathbb{R}, \tag{1}$$

where $\rho = \rho(t,x) \in \mathbb{R}_+$ is the conserved scalar quantity and $f\colon \mathbb{R}_+ \to \mathbb{R}_+$ is a Lipschitz continuous flux function [50]. Throughout the article, we suppose that f is a concave function.

The Cauchy problem to solve is then

$$\partial_t \rho + \partial_x f(\rho) = 0, \quad (t,x) \in \mathbb{R}_+ \times \mathbb{R}, \quad \rho(0,x) = \bar{\rho}(x), \quad x \in \mathbb{R}, \tag{2}$$

where $\bar{\rho}(x)$ is the initial condition. It can be shown that there exists a unique weak entropy solution for the Cauchy problem(2). For further details regarding the theory of hyperbolic conservation laws, we refer the reader to [1,51].

Definition 2.1 Riemann Problem. A Riemann problem is a Cauchy problem (2) with a piecewise-constant initial datum (called the Riemann datum):

$$\bar{\rho}(x) = \begin{cases} \rho_-, & \text{if } x < 0, \\ \rho_+, & \text{if } x \geq 0. \end{cases} \tag{3}$$

We denote the corresponding self-similar entropy weak solutions by $W_R\left(\frac{x}{t}; \rho_-, \rho_+\right)$.

2.2 Network of PDEs

A network is defined as a set of N links $\mathcal{I} = \{1, \ldots, N\}$, with junctions $\mathcal{J}$. Each junction $J \in \mathcal{J}$ is defined as the union of two nonempty sets: the set of

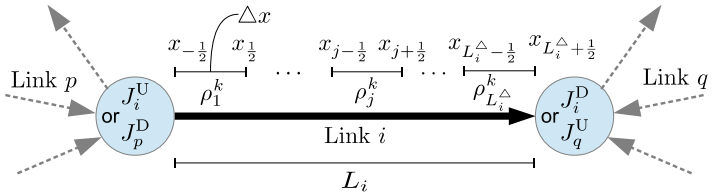

Fig. 1 Space discretization for a link $i \in \mathcal{I}$. Step size is uniform Δx, with discrete value ρ_j^k representing the state between x^{j-1} and x^j

n_J incoming links $\text{Inc}(J) = \left(i_J^1, \ldots, i_J^{n_J}\right) \subset \mathcal{I}$ and the set of m_J outgoing links $\text{Out}(J) = \left(i_J^{n_J+1}, \ldots, i_J^{n_J+m_J}\right) \subset \mathcal{I}$. Each link $i \in \mathcal{I}$ has an associated upstream junction $J_i^{\text{U}} \in \mathcal{J}$ and downstream junction $J_i^{\text{D}} \in \mathcal{J}$ and has an associated spatial domain $[0, L_i]$ over which the evolution of the state on link i, $\rho_i(t, x)$, solves the Cauchy problem:

$$(\rho_i)_t + f(\rho_i)_x = 0, \quad \rho_i(0, x) = \bar{\rho}_i(x), \tag{4}$$

where $\bar{\rho}_i \in BV \cap L^1_{\text{loc}}(L_i; \mathbb{R})$ is the initial condition on link i. For simplicity of notation, this section considers a single junction $J \in \mathcal{J}$ with $\text{Inc}(J) = (1, \ldots, n)$ and $\text{Out}(J) = (n+1, \ldots, n+m)$.

Remark 2.1 There is redundancy in the labeling of the junctions; if link i is directly upstream of link j, then we have $J_i^{\text{D}} = J_j^{\text{U}}$. See Fig. 1.

While the dynamics on each link $\rho_i(t, x)$ is determined by (4), the dynamics at junctions still needs to be defined.

Definition 2.2 Riemann problem at junctions. A Riemann problem at J is a Cauchy problem corresponding to an initial datum $(\bar{\rho}_1, \ldots, \bar{\rho}_{n+m}) \in \mathbb{R}^{n+m}$ which is constant on each link i.

Definition 2.3 A Riemann solver is a map that assigns a solution to each Riemann initial data. For each junction J it is a function

$$RS: \mathbb{R}^{m+n} \to \mathbb{R}^{m+n}, \quad (\bar{\rho}_1, \ldots, \bar{\rho}_{n+m}) \mapsto RS(\bar{\rho}_1, \ldots, \bar{\rho}_{n+m}) = \left(\hat{\rho}_1, \ldots, \hat{\rho}_{n+m}\right),$$

where $\hat{\rho}_i$ provides the trace for link i at the junction for all time $t \geq 0$.

For a link $i \in \text{Inc}(J)$, the solution $\rho_i(t, x)$ over its spatial domain $x < 0$ is given by the solution to the following Riemann problem:

$$(\rho_i)_t + f(\rho_i)_x = 0, \quad \rho_i(0, x) = \begin{cases} \bar{\rho}_i, & \text{if } x < 0, \\ \hat{\rho}_i, & \text{if } x \geq 0. \end{cases} \tag{5}$$

The Riemann problem for an outgoing link is defined similarly, with the following modifications:

$\rho_i(0, x > 0) = \bar{\rho}_i$ and $\rho_i(0, x \leq 0) = \hat{\rho}_i$. Note that the following properties for the Riemann Solver holds:

– All waves produced from the solution to Riemann problems must emanate out from the junction. In other words, the solution to the Riemann problem on an incoming link must only produce waves with negative speeds, while the solution on an outgoing link must only produce waves with positive speed.
– The sum of all incoming fluxes must equal the sum of all outgoing fluxes:

$$\sum_{i\in \mathrm{Inc}(J)} f\left(\hat{\rho}_i\right) = \sum_{j\in \mathrm{Out}(J)} f\left(\hat{\rho}_j\right). \tag{6}$$

This condition guarantees mass conservation at junctions.
– The Riemann solver must produce self-similar solutions, i.e.,

$$RS\left(RS\left(\bar{\rho}_1,\ldots,\bar{\rho}_{n+m}\right)\right) = RS\left(\bar{\rho}_1,\ldots,\bar{\rho}_{n+m}\right) = \left(\hat{\rho}_1,\ldots,\hat{\rho}_{n+m}\right). \tag{7}$$

The justification for these conditions can be found in [1]. The above conditions are not always sufficient to guarantee a unique Riemann solver. Additional conditions are added for specific applications to achieve uniqueness, often modeling additional physical phenomena at junctions. In Sect. 4, we detail the additional conditions added to the ramp metering solver which enforce flux maximization along the freeway mainline sections and specify a merging priority model for vehicles entering from the onramps.

2.3 Godunov Discretization

In order to find approximate solutions, we use the classical Godunov scheme [52]. We use the following notation: $x_{j+\frac{1}{2}}$ are the cell interfaces and $t^k = k\Delta t$ the time with $k \in \mathbb{N}$ and $j \in \mathbb{Z}$. x_j is the center of the cell, $\Delta x = x_{j+\frac{1}{2}} - x_{j-\frac{1}{2}}$ the cell width, and Δt is the time-step.

Godunov Scheme for a Single Link The Godunov scheme is based on the solutions of exact Riemann problems. The main idea of this method is to approximate the initial datum by a piecewise- constant function; then the resulting Riemann problems are solved exactly one time-step ahead and a global solution is constructed by piecing the problem solutions together. Finally, one takes the mean over each cell and proceeds by iteration. Given $\rho(t,x)$, the cell average of ρ at time t^k in the cell $C_j =]x_{j-\frac{1}{2}}, x_{j+\frac{1}{2}}]$ is given by

$$\rho_j^k = \frac{1}{\Delta x}\int_{x_{j-\frac{1}{2}}}^{x_{j+\frac{1}{2}}} \rho(t^k,x)dx. \tag{8}$$

Then we proceed as follows:

1. Solve the Riemann problem at each cell interface $x_{j+\frac{1}{2}}$ with initial data (ρ_j^k, ρ_{j+1}^k).
2. Compute the cell average at time t^{k+1} in each computational cell and obtain ρ_j^{k+1}.

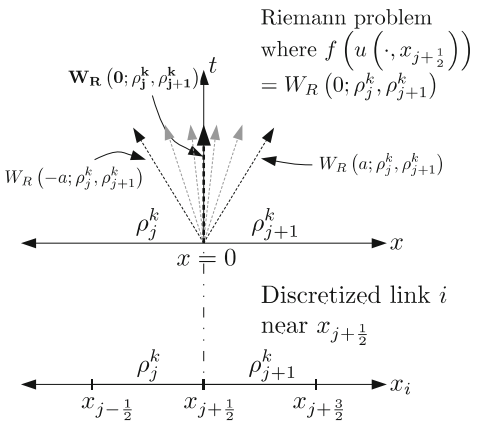

Fig. 2 Self-similar solution for Riemann problem with initial data (ρ_j^k, ρ_{j+1}^k). The self-similar solution at $\frac{x}{t} = 0$ for the top diagram [i.e., $W - R(0; p_j^k p_{j+1}^k)$] gives the flux solution to the discretized problem in the *bottom diagram*

We remark that waves in two neighboring cells do not intersect before Δt if the following Courant–Friedrichs–Lewy (CFL) condition holds, $\lambda^{\max} \leq \frac{\Delta x}{\Delta t}$, where $\lambda^{\max} = \max_a |f'(a)|$ is the maximum wave speed of the Riemann solution at the interfaces.

Godunov scheme can be expressed as follows:

$$\rho_j^{k+1} = \rho_j^k - \frac{\Delta t}{\Delta x}(g^G(\rho_j^k, \rho_{j+1}^k) - g^G(\rho_{j-1}^k, \rho_j^k)), \tag{9}$$

where g^G is the Godunov numerical flux given by

$$g^G : \mathbb{R} \times \mathbb{R} \to \mathbb{R}, (\rho_j, \rho_{j+1}) \mapsto g^G(\rho_j, \rho_{j+1}) = f(W_R(0; \rho_j, \rho_{j+1})),$$

where W_R is as defined in Definition 2.1. See Fig. 2 for a graphical depiction of W_R.

Godunov Scheme at Junctions The scheme just discussed applies to the case in which a single cell is adjacent to another single cell. Yet, at junctions, a cell may share a boundary with more than one cell. A more general Godunov flux can be derived for such cases. For incoming links near the junction, we have:

$$\rho_{L_i^\Delta}^{k+1} = \rho_{L_i^\Delta}^k - \frac{\Delta t}{\Delta x}\left(f\left(\hat{\rho}_{L_i^\Delta}^k\right) - g^G\left(\rho_{L_i^\Delta - 1}^k, \rho_{L_i^\Delta}^k\right)\right), \quad i \in \{1, \ldots, n\},$$

where L_i^Δ are the number of cells for link i (see Fig. 1) and $\hat{\rho}_i^k$ is the solution of the Riemann solver $RS\left(\rho_1^k, \ldots, \rho_{n+m}^k\right)$ for link i at the junction. The same can be done for the outgoing links:

$$\rho_1^{k+1} = \rho_1^k - \frac{\Delta t}{\Delta x}\left(g^G\left(\rho_1^k, \rho_2^k\right) - f\left(\hat{\rho}_1^k\right)\right), \quad i \in \{n+1, \ldots, n+m\}.$$

Remark 2.2 Using the Godunov scheme, each mesh grid at a given t^k can be seen as a node for a one-to-one junction with one incoming and one outgoing links. It is therefore more convenient to consider that every discretized cell is, rather, a link with both an upstream junction and downstream junction. Thus, we consider networks in which the state of each link $i \in \mathcal{I}$ at a time-step $k \in \{0, \ldots, T-1\}$ is represented by the single discrete value ρ_i^k.

The previous remark allows us to develop a generalized update step for all discrete state variables. We first introduce a definition in order to reduce the cumbersome nature of the preceding notation. Let the state variables adjacent to a junction $J \in \mathcal{J}$ at a time-step $k \in \{0, \ldots, T-1\}$ be represented as $\boldsymbol{\rho}_J^k := \left(\rho_{i_J^1}^k, \ldots, \rho_{i_J^{n_J+m_J}}^k\right)$. Similarly, we let the solution of a Riemann solver be represented as $\hat{\boldsymbol{\rho}}_J := RS\left(\boldsymbol{\rho}_J\right)$. Then, for a link $i \in \mathcal{I}$ with upstream and downstream junctions, J_i^{U} and J_i^{D}, and time-step $k \in \{0, \ldots, T-1\}$, the update step becomes:

$$\begin{aligned}\rho_i^{k+1} &= \rho_i^k - \frac{\Delta t}{\Delta x}\left(f\left(\left(RS\left(\boldsymbol{\rho}_{J_i^{\mathrm{D}}}^k\right)\right)_i\right) - f\left(\left(RS\left(\boldsymbol{\rho}_{J_i^{\mathrm{U}}}^k\right)\right)_i\right)\right)\\ &= \rho_i^k - \frac{\Delta t}{\Delta x}\left(f\left(\left(\hat{\boldsymbol{\rho}}_{J_i^{\mathrm{D}}}\right)_i\right) - f\left(\left(\hat{\boldsymbol{\rho}}_{J_i^{\mathrm{U}}}\right)_i\right)\right),\end{aligned} \tag{10}$$

where $(s)_i$ is the ith element of the tuple s. This equation is thus a general way of writing the Godunov scheme in a way, which applies everywhere, including at junctions.

Working Directly with Flux Solutions at Junctions The equations can be simplified if we do not explicitly represent the solution of the Riemann solver, $\hat{\boldsymbol{\rho}}_J$, and, instead, directly calculate the flux solution from the Riemann data. We denote this direct computation by g_J^G, the Godunov flux solution at a junction:

$$g_J^G : \mathbb{R}^{n_J+m_J} \to \mathbb{R}^{n_J+m_J}, \quad \boldsymbol{\rho}_J \mapsto f\left(RS\left(\boldsymbol{\rho}_J\right)\right) = \left(f\left(\hat{\rho}_1\right), \ldots, f\left(\hat{\rho}_{n+m}\right)\right). \tag{11}$$

This gives a simplified expressions for the update step:

$$\rho_i^{k+1} = \rho_i^k - \frac{\Delta t}{\Delta x}\left(\left(g_{J_i^{\mathrm{D}}}^G\left(\boldsymbol{\rho}_{J_i^{\mathrm{D}}}^k\right)\right)_i - \left(g_{J_i^{\mathrm{U}}}^G\left(\boldsymbol{\rho}_{J_i^{\mathrm{U}}}^k\right)\right)_i\right). \tag{12}$$

2.4 State, Control, and Governing Equations

The rest of the article focuses on controlling systems of the form in Eq. (12) in which some parts of the state can be controlled directly (for example, in the form of boundary control). We wish to solve the system in Eq. (12) T time-steps forward, i.e., we wish to determine the discrete state values ρ_i^k for all links $i \in \mathcal{I}$ and all time-steps $k \in \{0, \ldots, T-1\}$. Furthermore, at each time-step k, we assume a set of "control" variables $\left(u_1^k, \ldots, u_M^k\right) \in \mathbb{R}^M$ that influence the solution of the Riemann problems at junctions, where M is the number of controlled values at each time-step, and each

control may be updated at each time-step. We assume that a control may only influence a subset of junctions, which is a reasonable assumption if the controls have some spatial locality. Thus, for a junction $J \in \mathcal{J}$, we assume without loss of generality that a subset of the control parameters $\left(u^k_{j_J^1}, \ldots, u^k_{j_J^{M_J}}\right) \in \mathbb{R}^{M_J}$ influence the solution of the Riemann solver. Similar to the notation developed for state variables, for control variables, we define $\mathbf{u}^k_J := \left(u^k_{j_J^1}, \ldots, u^k_{j_J^{M_J}}\right)$ as the concatenation of the control variables around the junction J. To account for the addition of controls, we modify the Riemann problem at a junction $J \in \mathcal{J}$ at time-step k to be a function of the current state of connecting links $\boldsymbol{\rho}^k_J$, and the current control parameters $\mathbf{u}^k_J$. Then using the same notation as before, we express the Riemann solver as:

$$RS_J: \quad \mathbb{R}^{n_J+m_J} \times \mathbb{R}^{M_J} \to \mathbb{R}^{n_J+m_J}, \quad \left(\boldsymbol{\rho}^k_J, \mathbf{u}^k_J\right) \mapsto RS_J\left(\boldsymbol{\rho}^k_J, \mathbf{u}^k_J\right) = \hat{\boldsymbol{\rho}}^k_J.$$

We represent the entire state of the solved system with the vector $\boldsymbol{\rho} \in \mathbb{R}^{NT}$, where for $i \in \mathcal{I}$ and $k \in \{0, \ldots, T-1\}$, we have $\boldsymbol{\rho}_{Nk+i} = \rho^k_i$. Similarly, we represent the entire control vector by $\mathbf{u} \in \mathbb{R}^{MT}$, where $\mathbf{u}_{Mk+j} = u^k_j$. For each state variable ρ^k_i, write the corresponding update equation h^k_i:

$$h^k_i: \mathbb{R}^{NT} \times \mathbb{R}^{MT} \to \mathbb{R}, \quad (\boldsymbol{\rho}, \mathbf{u}) \mapsto h^k_i(\boldsymbol{\rho}, \mathbf{u}) = 0.$$

This takes the following form:

$$h^0_i(\boldsymbol{\rho}, \mathbf{u}) = \rho^0_i - \bar{\rho}_i = 0, \tag{13}$$

$$\begin{aligned} h^k_i(\boldsymbol{\rho}, \mathbf{u}) = \rho^k_i - \rho^{k-1}_i &+ \frac{\Delta t}{L_i} f\left(RS_{J_i^{\mathrm{D}}}\left(\boldsymbol{\rho}^{k-1}_{J_i^{\mathrm{D}}}, \mathbf{u}^{k-1}_{J_i^{\mathrm{D}}}\right)\right)_i \\ &- \frac{\Delta t}{L_i} f\left(RS_{J_i^{\mathrm{U}}}\left(\boldsymbol{\rho}^{k-1}_{J_i^{\mathrm{U}}}, \mathbf{u}^{k-1}_{J_i^{\mathrm{U}}}\right)\right)_i = 0 \quad \forall k \in \{2, \ldots, T-1\}, \end{aligned} \tag{14}$$

or in terms of the Godunov junction flux:

$$h^k_i(\boldsymbol{\rho}, \mathbf{u}) = \rho^k_i - \rho^{k-1}_i + \frac{\Delta t}{\Delta x}\left(g^G_{J_i^{\mathrm{D}}}\left(\boldsymbol{\rho}^k_{J_i^{\mathrm{D}}}, \mathbf{u}^{k-1}_{J_i^{\mathrm{D}}}\right)\right)_i - \frac{\Delta t}{\Delta x}\left(g^G_{J_i^{\mathrm{U}}}\left(\boldsymbol{\rho}^k_{J_i^{\mathrm{U}}}, \mathbf{u}^{k-1}_{J_i^{\mathrm{U}}}\right)\right)_i, \tag{15}$$

for all links $i \in \mathcal{I}$, where $\bar{\rho}_i$ is the initial condition for link i. Thus, we can construct a system of NT governing equations $H(\boldsymbol{\rho}, \mathbf{u}) = 0$, where the $h_{i,k}$ is the equation in H at index $Nk + i$; the ordering of $h_{i,k}$ matches that of the corresponding discrete state variable ρ^k_i.

3 Adjoint-Based Flow Optimization

3.1 Optimal Control Problem Formulation

In addition to our governing equations $H(\boldsymbol{\rho}, \mathbf{u}) = 0$, where we assume $h_i^k \in \mathcal{C}^1$, we introduce also a cost function $C \in \mathcal{C}^1$,

$$C\colon \mathbb{R}^{NT} \times \mathbb{R}^{MT} \to \mathbb{R}, \quad (\boldsymbol{\rho}, \mathbf{u}) \mapsto C(\boldsymbol{\rho}, \mathbf{u}),$$

which returns a scalar that serves as a metric of performance of the state and control values of the system. We wish to minimize the quantity C over the set of control parameters $\mathbf{u}$, while constraining the state of the system to satisfy the governing equations $H(\boldsymbol{\rho}, \mathbf{u}) = 0$, which is, again, the concatenated version of (14) or (15). We summarize this with the following optimization problem:

$$\min_{\mathbf{u}} C(\boldsymbol{\rho}, \mathbf{u}), \quad \text{s.t. } H(\boldsymbol{\rho}, \mathbf{u}) = 0. \tag{16}$$

Both the cost function and governing equations may be not convex in this problem.

3.2 Calculating the Gradient

We wish to use gradient information in order to find control values $\mathbf{u}^*$ that give locally optimal costs $C^* = C(\boldsymbol{\rho}(\mathbf{u}^*), \mathbf{u}^*)$. Since there may exist many local minima for this optimization problem (16) (which is not convex in general), gradient methods do not guarantee global optimality of $\mathbf{u}^*$. Still, nonlinear optimization methods such as interior point optimization utilize gradient information to improve performance [53]. In a descent algorithm, the optimization procedure will have to descend a cost function, by coupling the gradient, which, at a nominal point $(\boldsymbol{\rho}', \mathbf{u}')$ is given by:

$$d_{\mathbf{u}} C(\boldsymbol{\rho}', \mathbf{u}') = \left.\frac{\partial C(\boldsymbol{\rho}, \mathbf{u})}{\partial \boldsymbol{\rho}}\right|_{\boldsymbol{\rho}', \mathbf{u}'} \frac{\mathrm{d}\boldsymbol{\rho}}{\mathrm{d}\mathbf{u}} + \left.\frac{\partial C(\boldsymbol{\rho}, \mathbf{u})}{\partial \mathbf{u}}\right|_{\boldsymbol{\rho}', \mathbf{u}'}. \tag{17}$$

Remark 3.1 For Eq. (17) to be valid, all required partial and full derivatives must be well defined, including $\frac{\mathrm{d}\boldsymbol{\rho}}{\mathrm{d}\mathbf{u}}$. In some applications, this assumption does not necessarily hold, either because f itself is not smooth or because g^G is not smooth (and thus $H \notin \mathcal{C}^1$), as is the case for the LWR equation with concave fundamental diagrams. There are several settings in which the conditions for differentiability are satisfied; see in particular [9,54].

The main difficulty is to compute the term $\frac{\mathrm{d}\boldsymbol{\rho}}{\mathrm{d}\mathbf{u}}$. We take advantage of the fact that the derivative of $H(\boldsymbol{\rho}, \mathbf{u})$ with respect to $\mathbf{u}$ is equal to zero along trajectories of the system:

$$d_{\mathbf{u}} H(\boldsymbol{\rho}', \mathbf{u}') = \left.\frac{\partial H(\boldsymbol{\rho}, \mathbf{u})}{\partial \boldsymbol{\rho}}\right|_{\boldsymbol{\rho}', \mathbf{u}'} \frac{\mathrm{d}\boldsymbol{\rho}}{\mathrm{d}\mathbf{u}} + \left.\frac{\partial H(\boldsymbol{\rho}, \mathbf{u})}{\partial \mathbf{u}}\right|_{\boldsymbol{\rho}', \mathbf{u}'} = 0. \tag{18}$$

The partial derivative terms, $H_{\boldsymbol{\rho}} \in \mathbb{R}^{NT\times NT}$, $H_{\mathbf{u}} \in \mathbb{R}^{NT\times MT}$, $C_{\boldsymbol{\rho}} \in \mathbb{R}^{NT}$, and $C_{\mathbf{u}} \in \mathbb{R}^{MT}$, can all be evaluated (more details provided in Sect. 3.3) and then treated as constant matrices. Thus, in order to evaluate $d_{\mathbf{u}}C\left(\boldsymbol{\rho}', \mathbf{u}'\right) \in \mathbb{R}^{MT}$, we must solve a coupled system of matrix equations.

Forward System If we solve for $\frac{\mathrm{d}\boldsymbol{\rho}}{\mathrm{d}\mathbf{u}} \in \mathbb{R}^{NT\times MT}$ in (18), which we call the *forward system*:

$$H_{\boldsymbol{\rho}}\frac{\mathrm{d}\boldsymbol{\rho}}{\mathrm{d}\mathbf{u}} = -H_{\mathbf{u}}, \tag{19}$$

then we can substitute the solved value for $\frac{\mathrm{d}\boldsymbol{\rho}}{\mathrm{d}\mathbf{u}}$ into (17) to obtain the full expression for the gradient. Section 3.3 below gives details on the invertibility of $H_{\boldsymbol{\rho}}$, which guarantees a solution for $\frac{\mathrm{d}\boldsymbol{\rho}}{\mathrm{d}\mathbf{u}}$.

Adjoint System Instead of evaluating $\frac{\mathrm{d}\boldsymbol{\rho}}{\mathrm{d}\mathbf{u}}$ directly, the adjoint method solves the following system, called the adjoint system, for a new unknown variable $\lambda \in \mathbb{R}^{NT}$ (called the adjoint variable):

$$H_{\boldsymbol{\rho}}^T\lambda = -C_{\boldsymbol{\rho}}^T. \tag{20}$$

Under certain additional conditions on the flux function and discretization scheme, the adjoint system in Eq. (20) may be shown to converge to the continuous adjoint system as the discretization steps go toward zero, as described in the following works [9,22,30]. No such convergence results exist in our setting of using a Godunov discretization with general $n \times m$ junctions. The expression for the gradient becomes:

$$d_{\mathbf{u}}C\left(\boldsymbol{\rho}', \mathbf{u}'\right) = \lambda^T H_{\mathbf{u}} + C_{\mathbf{u}}. \tag{21}$$

We note that Eqs. (20) and (21) can be alternatively derived using the first-order *Karush–Kuhn–Tucker* (KKT) conditions, coupled with the constraint qualification in Eq. (16). Given we do not assume convexity of the underlying system, first-order KKT conditions are necessary, but not sufficient conditions for optimality of $\mathbf{u}$ and λ. For practical applications to nonconvex systems and for the purposes of this article, we do not necessarily seek global *or local* optimality, but rather the direction of steepest descent given in Eq. (21) in order to *improve* the performance of the system. We define $D_{\boldsymbol{\rho}}$ to be the maximum junction degree on the network:

$$D_{\boldsymbol{\rho}} = \max_{J\in\mathcal{J}}(n_J + m_J), \tag{22}$$

and also define $D_{\mathbf{u}}$ to be the maximum number of constraints in which a single control variable, which is equivalent to:

$$D_{\mathbf{u}} = \max_{u\in\mathbf{u}} \sum_{J\in\mathcal{J}:\, u\in\mathbf{u}_J^k} (n_J + m_J). \tag{23}$$

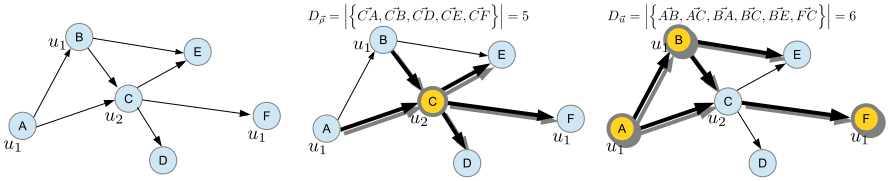

Fig. 3 Depiction of $D_{\boldsymbol{\rho}}$ and D_v for an arbitrary graph. **a** The underlying graphical structure for an arbitrary PDE network. Some control parameter u_1 has influence over junctions A, B, and F, while another control parameter u_2 has influence over only junction C. **b** The center junction having the largest number of connecting edges, thus giving $D_{\boldsymbol{\rho}} = 5$. **c** Control parameter u_1 influences three junctions with sum of junction degrees equal to six, which is maximal over the other control parameter u_2, leading to the result $D_{\mathbf{u}} = 6$. Note that in (**c**), the link going from junction A to junction B is counted twice: once as an outgoing link $\boldsymbol{AB}$ and once as in incoming link $\boldsymbol{BA}$

Note that $\left\{u \in \mathbf{u}_J^k \colon J \in \mathcal{J}\right\}$ is a k-dependent set. By convention, junctions are either actuated or not, so there is no dependency on k, i.e., if $\exists k$ s.t. $u \in \mathbf{u}_J^k$, then $\forall k, u \in \mathbf{u}_J^k$. Using these definitions, we show later in Sect. 3.4 how the complexity of computing the gradient is reduced from $O(D_{\boldsymbol{\rho}} N M T^2)$ to $O(T\left(D_{\boldsymbol{\rho}} N + D_{\mathbf{u}} M\right))$ by considering the adjoint method over the forward method. A graphical depiction of $D_{\boldsymbol{\rho}}$ and $D_{\mathbf{u}}$ are given in Fig. 3.

Freeway networks are usually considered to have topologies that are nearly planar, leading to junctions degrees which typically do not exceed 3 or 4, regardless of the total number of links. Also, from the locality argument for control variables in Sect. 2.4, a single control variable's influence over state variables will not grow with the size of the network. Thus, $D_{\boldsymbol{\rho}}$ and $D_{\mathbf{u}}$ are constant with respect to NT or MT for freeway networks, and gradient computations can be considered linear for the adjoint method.

3.3 Evaluating the Partial Derivatives

While no assumptions are made about the sparsity of the cost function C, the networked structure of the PDE system and the Godunov discretization scheme allows us to say more about the structure and sparsity of $H_{\boldsymbol{\rho}}$ and $H_{\mathbf{u}}$.

Partial Derivative Expressions Given that the governing equations require the evaluation of a Riemann solver at each step, we detail some of the necessary computational steps in evaluating the $H_{\boldsymbol{\rho}}$ and $H_{\mathbf{u}}$ matrices. If we consider a particular governing equation $h_i^k(\boldsymbol{\rho}, \mathbf{u}) = 0$, then we may determine the partial term with respect to $\rho_j^l \in \boldsymbol{\rho}$ by applying the chain rule:

$$\frac{\partial h_i^k}{\partial \rho_j^l} = \frac{\partial \rho_i^k}{\partial \rho_j^l} - \frac{\partial \rho_i^{k-1}}{\partial \rho_j^l} + \frac{\Delta t}{L_i} f'\left(RS_{J_i^{\mathrm{D}}}\left(\boldsymbol{\rho}_{J_i^{\mathrm{D}}}^{k-1}, \mathbf{u}_{J_i^{\mathrm{D}}}^{k-1}\right)_i\right) \frac{\partial}{\partial \rho_j^l}\left(RS_{J_i^{\mathrm{D}}}\left(\boldsymbol{\rho}_{J_i^{\mathrm{D}}}^{k-1}, \mathbf{u}_{J_i^{\mathrm{D}}}^{k-1}\right)_i\right) \tag{24}$$

$$- \frac{\Delta t}{L_i} f'\left(RS_{J_i^{\mathrm{U}}}\left(\boldsymbol{\rho}_{J_i^{\mathrm{U}}}^{k-1}, \mathbf{u}_{J_i^{\mathrm{U}}}^{k-1}\right)_i\right) \frac{\partial}{\partial \rho_j^l}\left(RS_{J_i^{\mathrm{U}}}\left(\boldsymbol{\rho}_{J_i^{\mathrm{U}}}^{k-1}, \mathbf{u}_{J_i^{\mathrm{U}}}^{k-1}\right)_i\right),$$

or if we consider the composed Riemann flux solver g_J^G in (11):

$$\frac{\partial h_i^k}{\partial \rho_j^l} = \frac{\partial \rho_i^k}{\partial \rho_j^l} - \frac{\partial \rho_i^{k-1}}{\partial \rho_j^l} + \frac{\Delta t}{L_i}\left(\frac{\partial}{\partial \rho_j^l}\left(g^G_{J_i^{\mathrm{D}}}\left(\boldsymbol{\rho}^{k-1}_{J_i^{\mathrm{D}}}, \mathbf{u}^{k-1}_{J_i^{\mathrm{D}}}\right)\right)_i - \frac{\partial}{\partial \rho_j^l}\left(g^G_{J_i^{\mathrm{U}}}\left(\boldsymbol{\rho}^{k-1}_{J_i^{\mathrm{U}}}, \mathbf{u}^{k-1}_{J_i^{\mathrm{U}}}\right)\right)_i\right). \tag{25}$$

A diagram of the structure of the $H_{\boldsymbol{\rho}}$ matrix is given in Fig. 4a. Similarly for $H_{\mathbf{u}}$, we take a control parameter $u_j^l \in \mathbf{u}$ and derive the expression:

$$\frac{\partial h_i^k}{\partial u_j^l} = +\frac{\Delta t}{L_i} f'\left(RS_{J_i^{\mathrm{D}}}\left(\boldsymbol{\rho}^{k-1}_{J_i^{\mathrm{D}}}, \mathbf{u}^{k-1}_{J_i^{\mathrm{D}}}\right)_i\right)\frac{\partial}{\partial u_j^l}\left(RS_{J_i^{\mathrm{D}}}\left(\boldsymbol{\rho}^{k-1}_{J_i^{\mathrm{D}}}, \mathbf{u}^{k-1}_{J_i^{\mathrm{D}}}\right)_i\right) - \frac{\Delta t}{L_i} f'\left(RS_{J_i^{\mathrm{U}}}\left(\boldsymbol{\rho}^{k-1}_{J_i^{\mathrm{U}}}, \mathbf{u}^{k-1}_{J_i^{\mathrm{U}}}\right)_i\right)\frac{\partial}{\partial u_j^l}\left(RS_{J_i^{\mathrm{U}}}\left(\boldsymbol{\rho}^{k-1}_{J_i^{\mathrm{U}}}, \mathbf{u}^{k-1}_{J_i^{\mathrm{U}}}\right)_i\right), \tag{26}$$

or for the composed Godunov junction flux solver g_J^G:

$$\frac{\partial h_i^k}{\partial u_j^l} = \frac{\Delta t}{L_i}\left(\frac{\partial}{\partial u_j^l}\left(g^G_{J_i^{\mathrm{D}}}\left(\boldsymbol{\rho}^{k-1}_{J_i^{\mathrm{D}}}, \mathbf{u}^{k-1}_{J_i^{\mathrm{D}}}\right)\right)_i - \frac{\partial}{\partial u_j^l}\left(g^G_{J_i^{\mathrm{U}}}\left(\boldsymbol{\rho}^{k-1}_{J_i^{\mathrm{U}}}, \mathbf{u}^{k-1}_{J_i^{\mathrm{U}}}\right)\right)_i\right). \tag{27}$$

Analyzing (24), the only partial terms that are not trivial to compute are $\frac{\partial}{\partial \rho_j^l}\left(RS_{J_i^{\mathrm{D}}}\left(\boldsymbol{\rho}^{k-1}_{J_i^{\mathrm{D}}}, \mathbf{u}^{k-1}_{J_i^{\mathrm{D}}}\right)_i\right)$ and $\frac{\partial}{\partial \rho_j^l}\left(RS_{J_i^{\mathrm{U}}}\left(\boldsymbol{\rho}^{k-1}_{J_i^{\mathrm{U}}}, \mathbf{u}^{k-1}_{J_i^{\mathrm{U}}}\right)_i\right)$. Similarly for (26), the only nontrivial terms are $\frac{\partial}{\partial u_j^l}\left(RS_{J_i^{\mathrm{D}}}\left(\boldsymbol{\rho}^{k-1}_{J_i^{\mathrm{D}}}, \mathbf{u}^{k-1}_{J_i^{\mathrm{D}}}\right)_i\right)$ and $\frac{\partial}{\partial u_j^l}\left(RS_{J_i^{\mathrm{U}}}\left(\boldsymbol{\rho}^{k-1}_{J_i^{\mathrm{U}}}, \mathbf{u}^{k-1}_{J_i^{\mathrm{U}}}\right)_i\right)$. Once one obtains the solutions to these partial terms, then one can construct the full $H_{\boldsymbol{\rho}}$ and $H_{\mathbf{u}}$ matrices and use (20) and (21) to obtain the gradient value. As these expressions are written for a general scalar conservation law, the only steps in computing the gradient that are specific to a particular conservation law and Riemann solver are computing the derivative of the flux function f and the partial derivative terms just discussed. These expressions are explicitly calculated for the problem of optimal ramp metering in Sect. 4.

3.4 Complexity of Solving Gradient via Forward Method Versus Adjoint Method

This section demonstrates the following proposition:

Proposition 3.1 *The total complexity for the adjoint method on a scalar hyperbolic network of PDEs is* $O(T\left(D_{\boldsymbol{\rho}}N + D_{\mathbf{u}}M\right))$.

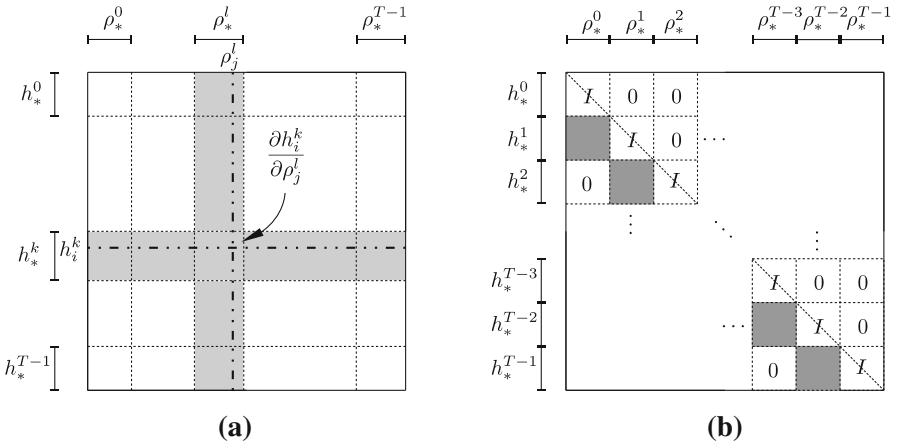

Fig. 4 Structure of the $H_{\boldsymbol{\rho}}$ matrix. **a** Ordering of partial derivative terms determined first by time, then cell index. **b** Sparsity structure of the $H_{\boldsymbol{\rho}}$ matrix. All blocks where $l \neq k-1$ are zero besides identity blocks on the diagonal

We can show the lower-triangular structure and invertibility of $H_{\boldsymbol{\rho}}$ by examining (13) and (14). For $k \in \{1, \ldots, T-1\}$, we have that h_i^k is only a function of ρ_i^k and of the state variables from the previous time-step $k-1$. Thus, based on our scheme in Sect. 2.4 for ordering variables by increasing time-step and ordering constraints by corresponding variable, we know that the diagonal terms of $H_{\boldsymbol{\rho}}$ are always 1 and all upper-triangular terms must be zero (since those terms correspond to constraints with a dependence of *future* values). These two conditions demonstrate both that $H_{\boldsymbol{\rho}}$ is lower-triangular and is invertible due to the ones along the diagonal. Additionally, if we consider taking partial derivatives with respect to the variable ρ_j^l, then we can deduce from Eq. (14) that all partial terms will be zero except for the diagonal term, and those terms involving constraints at time $j+1$ with links connecting to the downstream and upstream junctions J_j^{D} and J_j^{U} respectively. To summarize, $H_{\boldsymbol{\rho}}$ matrices for systems described in Sect. 2.4 will be square, invertible, lower-triangular, and each column will have a maximum cardinality equal to $D_{\boldsymbol{\rho}}$ in (22). The sparsity structure of $H_{\boldsymbol{\rho}}$ is depicted in Fig. 4b.

Using the same line of argument for the maximum cardinality of $H_{\boldsymbol{\rho}}$, we can bound the maximum cardinality of each column of $H_{\mathbf{u}}$. Taking a single control variable u_j^l, the variable can only appear in the constraints at time-step $j+1$ that correspond to a link that connects to a junction J such that $u_j^l \in \mathbf{u}_J^{l+1}$. These conditions give us the expression for $D_{\mathbf{u}}$ in (23), or the maximum cardinality over all columns in $H_{\mathbf{u}}$.

If we only consider the lower-triangular form of $H_{\boldsymbol{\rho}}$, then the complexity of solving for the gradient using the forward system is $O((NT)^2\, MT)$, where the dominating term comes from solving (17), which requires the solution of MT separate $NT \times NT$ lower-triangular systems. The lower-triangular system allows for forward substitution, which can be solved in $O((NT)^2)$ steps, giving the overall complexity $O((NT)^2\, MT)$. The complexity of computing the gradient via the adjoint method is $O((NT)^2 + (NT)\,(MT))$, which is certainly more efficient than the forward method, as long as $MT > 1$. The efficiency is gained by considering that (20) only requires the

solution of a single $NT \times NT$ *upper*-triangular system (via backward-substitution), followed by the multiplication of $\lambda^T H_v$, an $NT \times NT$ and an $NT \times MT$ matrix in (21), with a complexity of $O((NT)^2 + (NT)(MT))$.

For the adjoint method, this complexity can be improved upon by considering the sparsity of the $H_{\boldsymbol{\rho}}$ and $H_{\mathbf{u}}$ matrices, as detailed in Sect. 3.4. For the backward-substitution step, each entry in the λ vector is solved by *at most* $D_{\boldsymbol{\rho}}$ multiplications, and thus the complexity of solving (20) is reduced to $O(D_{\boldsymbol{\rho}} NT)$. Similarly, for the matrix multiplication of $\lambda^T H_v$, while λ is not necessarily sparse, we know that each entry in the resulting vector requires at most $D_{\mathbf{u}}$ multiplications, giving a complexity of $O(D_{\mathbf{u}} MT)$. Furthermore, if a sparse implementation of the $H_{\boldsymbol{\rho}}$ and $H_{\mathbf{u}}$ matrices are used, then memory usage will also scale linearly with the number of state and control variables.

4 Applications to Optimal Coordinated Ramp Metering on Freeways

4.1 Formulation of the Network Model and Explicit Riemann Solver

Model Consider a freeway section with links $\mathcal{I} = \{1, \ldots, 2N\}$ with a linear sequence of mainline links $= \{2, 4, \ldots, 2N\}$ and connecting on-ramp links $= \{1, 3, \ldots, 2N-1\}$. At discrete time $t = k\Delta t, 0 \leq k \leq T-1$, mainline link $2i \in \mathcal{I}, i \in \{1, \ldots, N\}$ has a downstream junction $J^{\mathrm{D}}_{2i} = J^{\mathrm{U}}_{2(i+1)}$ and an upstream junction $J^{\mathrm{U}}_{2i} = J^{\mathrm{D}}_{2(i-1)}$, while on-ramp $2i-1 \in \mathcal{I}, i \in \{1, \ldots, N\}$ has a downstream junction $J^{\mathrm{D}}_{2i-1} = J^{\mathrm{U}}_{2i} = J^{\mathrm{D}}_{2(i-1)}$ and an upstream junction J^{U}_{2i-1}. The off-ramp directly downstream of link $2i$ has, at time-step k, a split ratio β^k_{2i} representing the ratio of cars which stay on the freeway over the total cars leaving the upstream mainline of junction J^{D}_{2i}. The model assumes that all flux from on-ramp $2i-1$ enter downstream mainline $2i$. Since J^{U}_2 is the source of the network, it has no upstream mainline or off-ramp, and similarly J^{D}_{2N} has no downstream mainline or on-ramp ($\beta^k_{2N} = 0$). Each link $i \in \mathcal{I}$ has a discretized state value $\rho^k_i \in \mathbb{R}$ at each time-step $k \in \{0, \ldots, T-1\}$, that represents the density of vehicles on the link. These values are depicted in Fig. 5a. Junctions that have no on-ramps can be effectively represented by adding an on-ramp with no demand while junctions with no off-ramps can be represented by setting the split ratio to 1.

The vehicle flow dynamics on all links i (mainlines, on-ramps, and off-ramps) are modeled using the conservation law governing the density evolution (1), where ρ is the density state, and f is the flux function (or fundamental diagram) $f(\rho)$. In the context of traffic, this model is referred to as the Lighthill–Whitham–Richards (LWR) model [43,44]. The fundamental diagram f is typically assumed to be concave and has a bounded domain $\left[0, \rho^{\max}\right]$, and a maximum flux value $F^{\max}$ is attained at a critical density $\rho^c : f(\rho^c) = F^{\max}$. We assume that the fundamental diagram has a trapezoidal form parameterized by a free-flow speed v, congestion wave speed w, max flux $F^{\max}$, critical density ρ^c, and max density $\rho^{\max}$; see Fig. 5b. For the remainder of the article, we instantiate the conservation law in (1) with the LWR equation as it applies to traffic flow modeling.

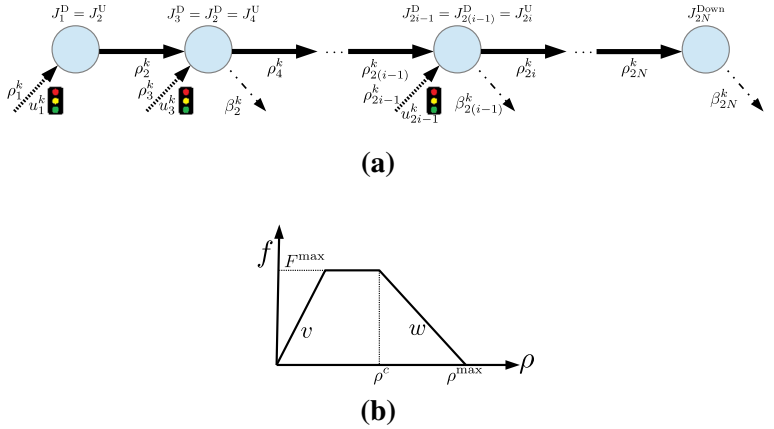

Fig. 5 Freeway network model and associated fundamental diagram. **a** Freeway network model. A junction $J^{\mathrm{D}}_{2i-1} = J^{\mathrm{D}}_{2(i-1)} = J^{\mathrm{U}}_{2i}$ at time k has associated densities $(\rho^k_{2(i-1)}, \rho^k_{2i}, \rho^k_{2i-1}, \beta^k_{2(i-1)})$ for the upstream mainline, downstream mainline, onramp and offramp split ratio, respectively. **b** Trapezoidal fundamental diagram

As control input, an on-ramp $2i-1 \in \mathcal{I},\ i \in \{1,\ldots,N\}$ at time-step $k \in \{0,\ldots,T-1\}$ has a metering rate $u^k_{2i-1} \in [0,1]$ which limits the flux of vehicles leaving the on-ramp. Intuitively, the metering rate acts as a fractional decrease in the flow leaving the on-ramp and entering the mainline freeway. The domain of the metering control is to force the control to neither impose negative flows nor send more vehicles than present in a queue. Its mathematical model is expressed in (33).

For notational simplicity, we define the set of densities of links incident to $J^{\mathrm{U}}_{2i} = J^{\mathrm{D}}_{2(i-1)}$ at time-step k as $\boldsymbol{\rho}^k_{J^{\mathrm{U}}_{2i}} = \left\{\rho^k_{2(i-1)}, \rho^k_{2i-1}, \rho^k_{2i}\right\}$. The off-ramp is considered to have infinite capacity, and thus has no bearing on the solution of junction problems. Initial conditions are handled as in (13), while for $k \in \{1,\ldots,T-1\}$, the mainline density ρ^k_{2i} using the Godunov scheme from (14) is given by:

$$\begin{aligned} h^k_{2i}(\boldsymbol{\rho},\mathbf{u}) &= \rho^k_{2i} - \rho^{k-1}_{2i} + \frac{\Delta t}{L_{2i}}\left(g^G_{J^{\mathrm{D}}_{2i}}\left(\boldsymbol{\rho}^{k-1}_{J^{\mathrm{D}}_{2i}}, u^{k-1}_{2i+1}\right)\right)_{2i} - \frac{\Delta t}{L_{2i}}\left(g^G_{J^{\mathrm{U}}_{2i}}\left(\boldsymbol{\rho}^{k-1}_{J^{\mathrm{U}}_{2i}}, u^{k-1}_{2i-1}\right)\right)_{2i} \\ &= \rho^k_{2i} - \rho^{k-1}_{2i} + \frac{\Delta t}{L_{2i}}\left(g^{k-1}_{2i,\mathrm{D}} - g^{k-1}_{2i,\mathrm{U}}\right) = 0, \end{aligned} \tag{28}$$

where we have introduced some substitutions to reduce the notational burden of this section: $g^k_{i,\mathrm{D}}$ is the Godunov flux at time-step k exiting a link i at the downstream boundary of the link, and $g^k_{i,\mathrm{U}}$ is the Godunov flux entering the link at the upstream boundary. We also make the assumption that on-ramps have infinite capacity and a free-flow velocity $v_{2i-1} = \frac{L_{2i-1}}{\Delta t}$ to prevent the ramp congestion from blocking demand from ever entering the network. Since the on-ramp has no physical length, the length is chosen arbitrarily and the "virtual" velocity chosen above is chosen to replicate the dynamics in [55]. We can then simplify the on-ramp update equation to be:

$$h^k_{2i-1}(\boldsymbol{\rho}, \mathbf{u}) = \rho^k_{2i-1} - \rho^{k-1}_{2i-1} - \frac{\Delta t}{L_{2i-1}} \left(\left(g^G_{J^{\mathrm{U}}_{2i}} \left(\boldsymbol{\rho}^{k-1}_{J^{\mathrm{U}}_{2i}}, u^{k-1}_{2i-1} \right) \right)_{2i-1} - D^{k-1}_{2i-1} \right) \tag{29}$$

$$= \rho^k_{2i-1} - \rho^{k-1}_{2i-1} - \frac{\Delta t}{L_{2i-1}} \left(g^{k-1}_{2i-1,\mathrm{D}} - D^{k-1}_{2i-1} \right) = 0, \tag{30}$$

where D^{k-1}_{2i-1} is the on-ramp *flux* demand, and the same notational simplification has been used for the downstream flux. This formulation results in "strong" boundary conditions at the on-ramps which guarantees all demand enters the network. Details on weak versus strong boundary conditions can be found in [2,55]. The on-ramp model in (29) differs from [55] in that we model the on-ramp as a discretized PDE with an infinite critical density, while [55] models the on-ramp as an ODE "buffer". While both models implement strong boundary conditions, the discretized PDE model makes the freeway network more aligned with the PDE network framework presented in this article.

Riemann Solver For the ramp metering problem, there are many potential Riemann solvers that satisfy the properties required in Sect. 2.2. Following the model of [55], for each junction J^{U}_{2i}, we add two modeling decisions: **(1)** the flux solution maximizes the outgoing mainline flux $g^k_{2i,\mathrm{U}}$ and **(2)** the flux solution attempts to satisfy $g^k_{2(i-1),\mathrm{D}} = p_{2(i-1)} g^k_{2i-1,\mathrm{D}}$ subject to **(1)**, where $p_{2(i-1)} \in \mathbb{R}_+$ is a merging parameter for junction $J^{\mathrm{D}}_{2(i-1)}$. Since **(1)** allows multiple flux solutions at the junction, **(2)** is necessary to obtain a unique solution. This leads to the following system of equations that gives the flux solution of the Riemann solver at time-step $k \in \{1, \ldots, T-1\}$ and junction J^{U}_{2i} for $i \in \{1, \ldots, N\}$:

$$\delta^k_{2(i-1)} = \min \left(v_{2(i-1)} \rho^k_{2(i-1)}, F^{\max}_{2(i-1)} \right) \tag{31}$$

$$\sigma^k_{2i} = \min \left(w_{2i} \left(\rho^{\max}_{2i} - \rho^k_{2i} \right), F^{\max}_{2i} \right) \tag{32}$$

$$d^k_{2i-1} = u^k_{2i-1} \min \left(\frac{L_{2i-1}}{\Delta t} \rho^k_{2i-1}, F^{\max}_{2i-1} \right) \tag{33}$$

$$g^k_{2i,\mathrm{U}} = \min \left(\beta^k_{2(i-1)} \delta^k_{2(i-1)} + d^k_{2i-1}, \sigma^k_{2i} \right) \tag{34}$$

$$g^k_{2(i-1),\mathrm{D}} = \begin{cases} \delta^k_{2(i-1)}, & \text{if } \frac{p_{2(i-1)} g^k_{2i,\mathrm{U}}}{\beta^k_{2(i-1)}(1+p_{2(i-1)})} \geq \delta^k_{2(i-1)} \quad \text{[Case 1]} \\ \frac{g^k_{2i,\mathrm{U}} - d^k_{2i-1}}{\beta^k_{2(i-1)}}, & \text{if } \frac{g^k_{2i,\mathrm{U}}}{1+p_{2(i-1)}} \geq d^k_{2i-1} \quad \text{[Case 2]} \\ \frac{p_{2(i-1)} g^k_{2i,\mathrm{U}}}{(1+p_{2(i-1)})\beta^k_{2(i-1)}}, & \text{otherwise} \quad \text{[Case 3]} \end{cases} \tag{35}$$

$$g^k_{2i-1,\mathrm{D}} = g^k_{2i,\mathrm{U}} - \beta^k_{2(i-1)} g^k_{2(i-1),\mathrm{D}}. \tag{36}$$

For notational simplicity, at the edges of the range for i, any undefined state values (e.g., ρ^k_0) are assumed to be zero by convention. Equations (31) and (33) determine the

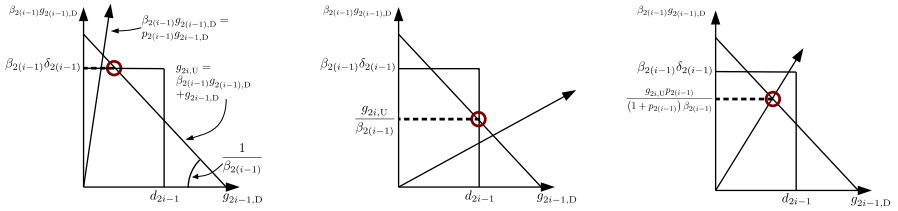

Fig. 6 Godunov junction flux solution for ramp metering model at junction J_{2i}^{U}. The *rectangular region* represents the feasible flux values for $\beta_{2(i-1)}g_{2(i-1),\mathrm{D}}$ and $g_{2i-1,\mathrm{D}}$ as determined by the upstream demand, while the line with slope $\frac{1}{\beta_{2(i-1)}}$ represents feasible flux values as determined by mass balance. The $\beta_{2(i-1)}g_{2(i-1),\mathrm{D}}$ term accounts for only the flux out of link $2\,(i-1)$ that stays on the mainline. The flux solution, represented by the *red circle*, is the point on the feasible region that minimizes the distance from the priority line $\beta_{2(i-1)}g_{2(i-1),\mathrm{D}} = p_{2(i-1)}g_{2i-1,\mathrm{D}}$. **a** Case 1: Priority violated due to limited upstream mainline demand entering downstream mainline. **b** Case 2: Priority violated due to limited on-ramp demand entering downstream mainline. **c** Case 3: Priority rule satisfied due to sufficient demand from both mainline and on-ramp

maximum flux that can exit link $2(i-1)$ and link $2i-1$ respectively. Equation (32) gives the maximum flux allowed into link $2i$. The actual flux into link $2i$, shown in (34), is given as the minimum of the "demand" from upstream links and "supply" of the downstream link. See [55] for more details on the model for this equation. The flux out of link $2(i-1)$ is split into three cases in (35). The solutions are depicted in Fig. 6, which demonstrates how the flux solution depends upon the respective demands and the merging parameter $p_{2(i-1)}$. Finally, Eq. (36) gives the flux out of the on-ramp $2i-1$, which is the difference between the flux into link $2i$ and the flux out of link $2\,(i-1)$ the remains on the mainline. For $k=0$, the update equation is given by a pre-specified initial condition, as in (13). Note that the equations can be solved sequentially via forward substitution. Also, we do not include the flux result for off-ramps explicitly here since its value has no bearing on further calculations, and we will henceforth ignore its calculation. To demonstrate that indeed the flux solution satisfies the flux conservation property, the off-ramp flux is trivially determined to be $\beta_{2(i-1)}^{k}g_{2(i-1),\mathrm{D}}^{k}$.

4.2 Formulation of the Optimal Control Problem

Optimal Coordinated Ramp Metering Combining (13) with (28) and (29) gives a complete description of the system $H(\boldsymbol{\rho},\mathbf{u})=0$, $\boldsymbol{\rho}\in\mathbb{R}^{2N}$, $\mathbf{u}\in\mathbb{R}$, where:

$$\begin{aligned}\boldsymbol{\rho}_{2Nk+i} &:= \rho_i^k, \quad 1\le i\le 2N, 0\le k\le T-1,\\ \mathbf{u}_{Nk+i} &:= u_{2i}^k, \quad 1\le i\le N, 0\le k\le T-1.\end{aligned}$$

The objective of the control is to minimize the *total travel time* on the network, expressed by the cost function C:

$$C(\boldsymbol{\rho}, \mathbf{u}) = \Delta t \sum_{k=1}^{T} \sum_{i=1}^{2N} L_i \rho_i^k. \tag{37}$$

The optimal coordinated ramp metering problem can be formulated as an optimization problem with PDE network constraints:

$$\min_{\mathbf{u}} C(\boldsymbol{\rho}, \mathbf{u}), \quad \text{s.t. } H(\boldsymbol{\rho}, \mathbf{u}) = 0, \quad 0 \le u \le 1, \quad \forall u \in \mathbf{u}. \tag{38}$$

Standard methods exist for the handling of geometric constraints on $\mathbf{u}$ in descent methods [such as the box constraints on $\mathbf{u}$ in Eq. (38)], such as projection methods [40] and barrier methods [10,56,57].

Applying the Adjoint Method To use the adjoint method as described in Sect. 3, we need to compute the partial derivative matrices $H_{\boldsymbol{\rho}}$, $H_{\mathbf{u}}$, $\tilde{C}_{\boldsymbol{\rho}}$ and $\tilde{C}_{\mathbf{u}}$. Computing the partial derivatives with respect to the cost function and box log-barrier terms is straightforward:

$$\frac{\partial \tilde{C}}{\partial \rho_i^k} = \Delta t L_i, \quad 1 \le i \le 2N, 0 \le k \le T-1,$$
$$\frac{\partial \tilde{C}}{\partial u_{2i}^k} = \epsilon \left(\frac{1}{1-u_{2i}^k} - \frac{1}{u_{2i}^k} \right), \quad 1 \le i \le N, 0 \le k \le T-1.$$

To compute the partial derivatives of H, we follow the procedure in Sect. 3.2. For an upstream junction $J_{2i}^{\mathrm{U}} \in \mathcal{J}$ and time-step $k \in \{1, \ldots, T-1\}$, we only need to compute the partial derivatives of the flux solver $g_{J_{2i}^{\mathrm{U}}}^{G}\left(\boldsymbol{\rho}_{J_{2i}^{\mathrm{U}}}^k, u_{2i-1}^k\right)$ with respect to the adjacent state variables $\boldsymbol{\rho}_{J_i}^k$ and ramp metering control u_i^k. We calculate the partial derivatives of the functions in (31)–(36) with respect to either a state or control variable $s \in \boldsymbol{\rho} \cup \mathbf{u}$:

$$\frac{\partial \delta_{2(i-1)}^k}{\partial s} = \begin{cases} v_{2(i-1)}, & \text{if } s = \rho_{2(i-1)}^k, v_i \rho_{2(i-1)}^k \le F_{2(i-1)}^{\max} \\ 0 & \text{otherwise} \end{cases},$$
$$\frac{\partial \sigma_{2i}^k}{\partial s} = \begin{cases} -w_{2i}, & \text{if } s = \rho_{2i}^k, w_{2i}\left(\rho_{2i}^{\max} - \rho_{2i}^k\right) \le F_{2i}^{\max} \\ 0 & \text{otherwise} \end{cases},$$
$$\frac{\partial d}{\partial s} = \begin{cases} u_{2i-1}^k, & \text{if } s = \rho_{2i-1}^k, \rho_{2i-1}^k \le F_{2i-1}^{\max} \\ \min\left(\rho_{2i-1}^k, F_{2i-1}^{\max}\right), & \text{if } s = u_{2i-1}^k \\ 0 & \text{otherwise} \end{cases},$$
$$\frac{\partial}{\partial s} g_{2i,\mathrm{U}}^k = \begin{cases} \beta_{2(i-1)}^k \frac{\partial \delta_{2(i-1)}^k}{\partial s} + \frac{\partial d_{2(i-1)}^k}{\partial s}, & \text{if } \beta_{2(i-1)}^k \delta_{2(i-1)}^k + d_{2i-1}^k \le \sigma_{2i}^k \\ \frac{\partial \sigma_{2i}^k}{\partial s} & \text{otherwise} \end{cases},$$

$$\frac{\partial}{\partial s} g_{2(i-1),\mathrm{D}} = \begin{cases} \frac{\partial \delta^k_{2(i-1)}}{\partial s}, & \text{if } \frac{g^k_{2i,\mathrm{U}} p_{2(i-1)}}{1+p_{2(i-1)}} \geq \frac{\delta^k_{2(i-1)}}{\beta^k_{2(i-1)}} \\ \frac{1}{\beta^k_{2(i-1)}} \left(\frac{\partial}{\partial s} g^k_{2i,\mathrm{U}} - \frac{\partial d^k_{2i-1}}{\partial s} \right), & \text{if } \frac{g^k_{2i,\mathrm{U}}}{1+p_{2(i-1)}} \geq d^k_{2(i-1)}, \\ \frac{p_{2(i-1)}}{\beta^k_{2(i-1)}(1+p_{2(i-1)})} \frac{\partial}{\partial s} g^k_{2i,\mathrm{U}} & \text{otherwise} \end{cases}$$

$$\frac{\partial}{\partial s} g_{2i-1,\mathrm{D}} = \frac{\partial}{\partial s} g^k_{2i,\mathrm{U}} - \beta^k_{2(i-1)} \frac{\partial}{\partial s} g_{2(i-1),\mathrm{D}}.$$

These expressions fully quantify the partial derivative values needed in (25) and (27). Thus we can construct the $H_{\boldsymbol{\rho}}$ and $H_{\mathbf{u}}$ matrices. With these matrices and $C_{\boldsymbol{\rho}}$ and $C_{\mathbf{u}}$, we can solve for the adjoint variable $\lambda \in \mathbb{R}^{2NT}$ in (20) and substitute its value into (21) to obtain the gradient of the cost function C with respect to the control parameter $\mathbf{u}$.

5 Numerical Results for Model Predictive Control Implementations

To demonstrate the effectiveness of using the adjoint ramp metering method to compute gradients, we implemented the algorithm on practical scenarios with field experimental data. The algorithm is useful as a gradient computation subroutine inside any descent-method optimization solver that takes advantage of first-order gradient information. Our implementation makes use of the open-source *IpOpt* solver [53], an interior point, nonlinear program optimizer. To serve as comparisons, two other case scenarios were run:

1. No control: the metering rate is set to 1 on all on-ramps at all times.
2. Alinea [46]: a well-adopted, feedback-based ramp metering algorithm commonly used by practitioners. Alinea is computationally efficient and decentralized, making it a popular choice for large networks, but does not take estimated boundary flow data as input. Since Alinea has a number of tuning parameters, we perform a *modified* grid-search technique over the different parameters that scales linearly with the number of on-ramps, and select the best-performing parameters. A *full* grid-search approach scales exponentially with the number of on-ramps, which is computationally infeasible for moderate-sized freeway networks.

All simulations were run on a 2012 commercial laptop with 8 GB of RAM and a dual-core 1.8 GHz Intel Core i5 processor.

Remark 5.1 We also implemented gradient descent using a finite differences approach similar to [41], which requires an $O(T^2NM)$ computation for each gradient step. The method was shown to be infeasible for real-time applications, taking over 1 min to compute a gradient step for a four link network over six time-steps. We thus do not consider finite differences in our subsequent numerical studies.

5.1 Implementation of I15S in San Diego

We constructed a model of a 19.4-mile stretch of the I15 South freeway in San Diego, California between San Marcos and Mira Mesa. The network has $N = 125$ links, and

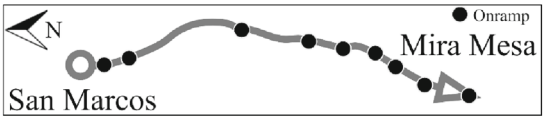

(a)

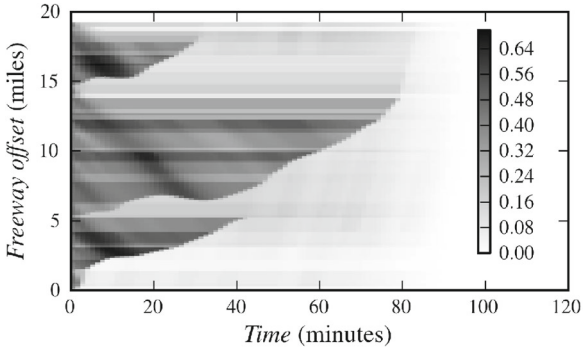

(b)

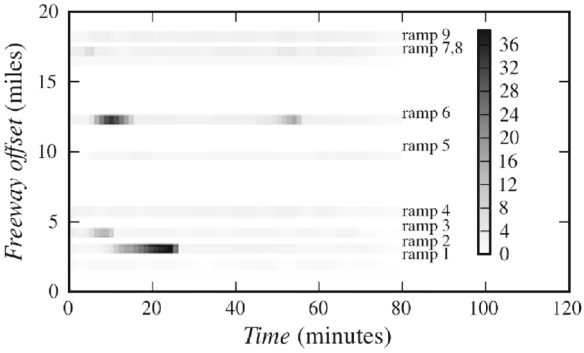

(c)

Fig. 7 Density and queue profile of no-control simulation of I15 freeway model (**a**). In 80 min, congestion pockets form on the freeway and queues form on the on-ramps, eventually clearing after 120 min. **a** Model of 19.4 mile (125 link), 9 on-ramp section of I15 South in San Diego, California. **b** Density profile. The units are the ratio of a link's vehicle density to a link's jam density. **c** On-ramp queue profile in units of vehicles

$M = 9$ on-ramps, with boundary data specified for $T = 1800$ time-steps, for a time horizon of 120 min given $\Delta t = 4$ s. The network is shown in Fig. 7a. Link length data was obtained using the Scenario Editor software developed as part of the *Connected Corridors* project, a collaboration between UC Berkeley and PATH research institute in Berkeley, California. Fundamental diagram parameters, split ratios, and boundary data were also obtained using calibration techniques developed by Connected Corridors. Densities resulting in free-flow speeds were chosen as initial conditions on the mainline and on-ramps. The data used in calibration were taken from PeMS sensor data [58]

during a morning rush hour period, scaled to generate congested conditions. The input data were chosen to demonstrate the effectiveness of the adjoint ramp metering method in a real-world setting. A profile of the mainline and on-ramps during a forward simulation of the network is shown in Fig. 7 under the described boundary conditions.

5.2 Finite-Horizon Optimal Control

Experimental Setup The adjoint ramp metering algorithm is compared to the reactive Alinea scheme, for which we assume that perfect boundary conditions and initial conditions are available. The metric we use to compare the different strategies is *reduced congestion* percentage, $\bar{c} \in]-\infty, 100]$, which we define as $\bar{c} = 100\left(1 - \frac{c_c}{c_{nc}}\right)$, where $c_c, c_{nc} \in \mathbb{R}_+$ are the *congestion* resulting from the *control* and *no-control* scenarios, respectively. We use the metric for congestion as defined in [59]; for a given section of road S and time horizon T, the congestion is given as

$$c(S,T) = \sum_{(s\in S,\tau\in T)} \max\left[\mathrm{TTT}(s,\tau) - \frac{\mathrm{VMT}(s,\tau)}{v_s}, 0\right], \tag{39}$$

where v_s is the free-flow velocity, VMT is total vehicle miles traveled, and TTT is total travel time over the link s and time-step τ. Since it is infeasible to compute the global optimum for all cases, a reduced congestion of 100 % serves as an upper bound on the possible amount of improvement.

Results Figure 8a, b shows the difference in density and on-ramp queue lengths between the no-control and adjoint-based controller simulations. The adjoint method was successful in appropriately deciding which ramps should be metered in order to improve throughput for the mainline. Running time analysis shows that the adjoint method can produce beneficial results in real-time applications. Figure 8c details the improvement in the adjoint method as a function of the overall running time of the algorithm. After just a few gradient steps, the adjoint method outperforms the Alinea method. Given that the time horizon of 2 h is longer than the period of time one can expect reasonably accurate boundary flow estimates, more practical simulations with shorter time horizons should permit more gradient steps in a real-time setting. While the adjoint method leads to queues with a considerable number of cars in some on-ramps, this can be addressed by introducing barrier terms into the cost function that limit the maximum queue length. The Alinea method tested for the I15 network had no prescribed maximum queue lengths as well, but was not able to produce significant improvements in total travel time reduction, while the adjoint method was more successful.

5.3 Model Predictive Control

To study the performance of the algorithm under noisy input data, we embed both the adjoint ramp metering algorithm and the Alinea algorithm inside of a *model predictive control* (MPC) loop.

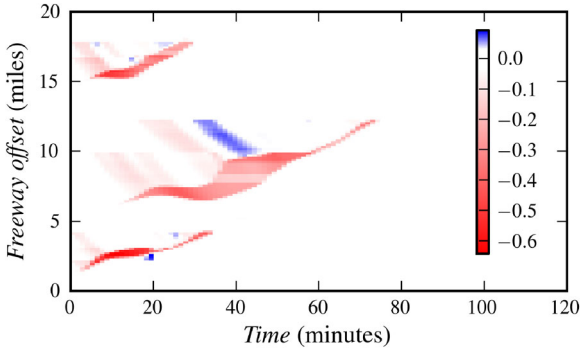

(a)

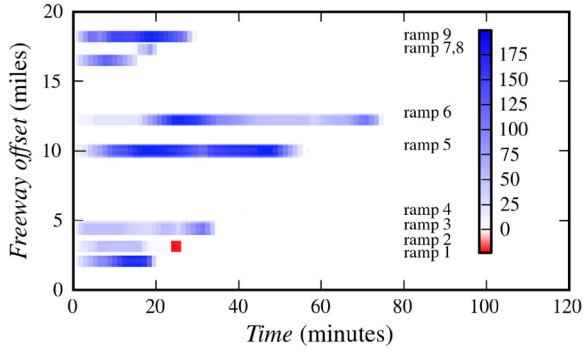

(b)

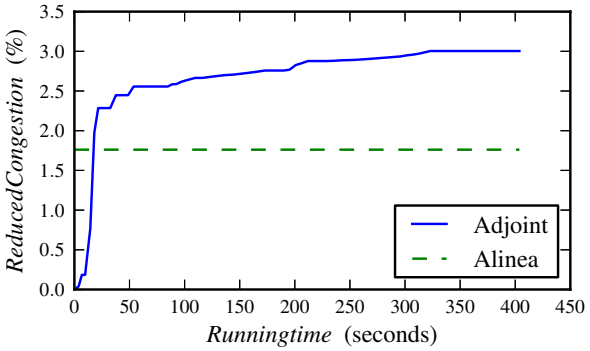

(c)

Fig. 8 Space–time vehicle density profiles and running time comparison. *View in color.* **a** Density difference ($\frac{\text{veh.}}{\text{m}}$) between the control and no-control scenario, normalized by jam density. **b** Queue difference profile in units of vehicles. **c** Comparison of reduced congestion versus simulation time between adjoint method and Alinea

Experimental Setup The MPC loop begins at a time t by estimating the initial conditions of the traffic on the freeway network and the predicted boundary fluxes over a certain time horizon T_h. These values are noisy, as exact estimation of these parameters is not possible on real freeway networks. The estimated conditions are then passed to the ramp metering algorithm to compute an optimal control policy over the T_h time period. The system is then forward-simulated over an update period of $T_u \leq T_h$, using the exact initial conditions and boundary conditions, as opposed to the noisy data used to compute control parameters. The state of the system and boundary conditions at $t + T_u$ are then estimated (with noise), and the process is repeated. A nonnegative *noise factor*, $\sigma \in \mathbb{R}_+$, is used to study how the adjoint method and Alinea perform as the quality of estimated data decreases. If ρ is the actual density for a cell and time-step, then the density $\bar{\rho}$ passed to the control schemes is given by:

$$\bar{\rho} = \rho \cdot (1 + \sigma \cdot R), \tag{40}$$

where R is a uniformly distributed random variable with mean 0 and domain $[-0.5, 0.5]$. The noise factor was applied to both initial and boundary conditions. Two different experiments were conducted:

1. Real-time I15 South: MPC is run for the I15 South network with $T_h = 80$ min and $T_u = 26$ min. A noise factor of 2 % was chosen for the initial and boundary conditions. The number of iterations was chosen in order to ensure that each MPC iteration finished in the predetermined update time T_u.
2. Noise Robustness: MPC is for over a synthetic network with length 12 miles and boundary conditions over 75 min. The experiments are run over a profile of noise factors between 1 and 8000 %.

Results **Real-Time I15 South** The results are summarized in Fig. 9a. The adjoint method applied once to the entire horizon with perfect boundary and initial condition information serves as a baseline performance for the other simulations, which had noisy input data and limited knowledge of predicted boundary conditions. The adjoint method still performs well under the more realistic conditions of the MPC loop with

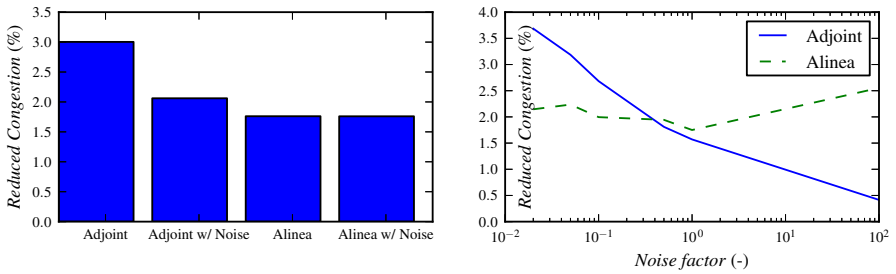

Fig. 9 Summary of model predictive control simulations. The results indicate that the adjoint method has superior performance for moderate noise levels on the initial and boundary conditions. **a** Reduced congestion. **b** Reduced congestion with increasing sensor noise for network with synthetic data

noise, resulting in 2 % reduced congestion or 40 car-hours in relation to no control, as compared to the 3 % reduced (60 car-hours) congestion achieved by the adjoint method with no noise and full time horizon ($T_h = T$). In comparison, the Alinea method was only able to achieve 1.5 % reduced congestion (30 car-hours) for both the noisy and no-noise scenarios. The results indicate that, under a realistic assumption of a 2 % noise factor in the sensor information, the algorithm's ability to consider boundary conditions results in an improvement upon strictly reactive policies, such as Alinea.

Robustness to Noise Simulation results on the synthetic network with varying levels of noise are shown in Fig. 9b. The adjoint method is able to outperform the Alinea method when the noise level is less than 80 %, a reasonable assumption for data provided by well-maintained loop detectors. As the initial and boundary condition data deteriorate, the adjoint method becomes useless. Since Alinea does not rely on boundary data, it is able to produce improvements, even with severely noisy data. The results indicate that the adjoint method will outperform Alinea under reasonable noise levels in the sensor data.

6 Conclusions

This article has detailed a simple framework for finite-horizon optimal control methods on a network of scalar conservation laws derived from first discretizing the network via the Godunov method, then applying the discrete adjoint to this system. Furthermore, we show that for this class of problems, the sparsity pattern allows the problem to be implemented with only linear memory and linear computational complexity with respect to the number of state and control parameters. We demonstrate the scalability of the approach by implementing a coordinated ramp metering algorithm using the adjoint method and applying the algorithm to the I-15 South freeway in California. The algorithm runs in a fraction of real-time and produces significant improvements over existing algorithms. A key benefit of the framework is its generality to other network control problems, particularly traffic systems. Variable speed limit control and parameter calibration [14] can be formulated in the same adjoint framework as ramp metering, with only a few modifications to the partial derivative matrices. As part of future work, we hope to demonstrate the wider applicability of the discrete adjoint method in traffic systems by developing variable speed limit and optimal rerouting of traffic algorithms based on the presented framework. For real-time applications, the numerical methods presented scaled well to a single freeway of real-world size. To enable larger-scale coordination of control schemes, more work needs to be done into the parallelization of adjoint-based approaches. As future work, we are investigating decentralized, coordinated control schemes over physical networks via the adjoint method. Such an approach would allow sub-networks to efficiently compute local policies using our presented framework, while constructing communication schemes across the sub-networks to enable performance of the combined networks to converge to a global optimum.

Acknowledgments The authors have been supported by the California Department of Transportation under the Connected Corridors program, CAREER Grant CNS-0845076 under the project 'Lagrangian Sensing in Large Scale Cyber-Physical Infrastructure Systems', the European Research Council under the

European Union's Seventh Framework Program (FP/2007-2013)/ERC Grant Agreement No. 257661, the INRIA associated team 'Optimal REroute Strategies for Traffic managEment' and the France-Berkeley Fund under the project 'Optimal Traffic Flow Management with GPS Enabled Smartphones'.

References

1. Garavello, M., Piccoli, B.: Traffic Flow on Networks, vol. 1. American Institute of Mathematical Sciences, Springfield (2006)
2. Work, D.B., Blandin, S., Tossavainen, O.P., Piccoli, B., Bayen, A.M.: A traffic model for velocity data assimilation. Appl. Math. Res. eXpress **2010**(1), 1 (2010)
3. Frazzoli, E., Dahleh, M.A., Feron, E.: Real-time motion planning for agile autonomous vehicles. J. Guid. Control Dyn. **25**(1), 116–129 (2002)
4. Brunnermeier, S., Martin, S.: Interoperability cost analysis of the US automotive supply chain: final report. Technical report, DIANE Publishing (1999)
5. Gugat, M., Dick, M., Leugering, G.: Gas flow in fan-shaped networks: classical solutions and feedback stabilization. SIAM J. Control Optim. **49**(5), 2101–2117 (2011)
6. Rothfarb, B., Frank, H., Rosenbaum, D.M., Steiglitz, K., Kleitman, D.J.: Optimal design of offshore natural-gas pipeline systems. Oper. Res. **18**(6), 992–1020 (1970)
7. Gugat, M.: Contamination source determination in water distribution networks. SIAM J. Appl. Math. **72**(6), 1772–1791 (2012)
8. Rabbani, T.S., Meglio, F.D., Litrico, X., Bayen, A.M.: Feed-forward control of open channel flow using differential flatness. IEEE Trans. Control Syst. Technol. **18**(1), 213–221 (2010)
9. Gugat, M., Herty, M., Klar, A., Leugering, G.: Optimal control for traffic flow networks. J. Optim. Theory Appl. **126**(3), 589–616 (2005)
10. Bayen, A., Raffard, R., Tomlin, C.: Adjoint-based control of a new eulerian network model of air traffic flow. IEEE Trans. Control Syst. Technol. **14**(5), 804–818 (2006)
11. Kotsialos, A., Papageorgiou, M.: Nonlinear optimal control applied to coordinated ramp metering. IEEE Trans. Control Syst. Technol. **12**(6), 920–933 (2004)
12. Coron, J.M., Vazquez, R., Krstic, M., Bastin, G.: Local exponential H 2 stabilization of a 2×2 quasilinear hyperbolic system using backstepping. SIAM J. Control Optim. **51**(3), 2005–2035 (2013)
13. Glass, O., Guerrero, S.: On the uniform controllability of the Burgers equation. SIAM J. Control Optim. **46**(4), 1211–1238 (2007)
14. Jacquet, D., Krstic, M., de Wit, C.C.: Optimal control of scalar one-dimensional conservation laws. In: American Control Conference, vol. 2, p. 6. IEEE (2006)
15. Blanchard, L., Duvigneau, R., Vuong, A.V., Simeon, B.: Shape gradient for isogeometric structural design. J. Optim. Theory Appl. **161**(2), 361–367 (2014)
16. Keller, D.: Optimal control of a nonlinear stochastic schrödinger equation. J. Optim. Theory Appl. 1–12 (2013). doi:10.1007/s10957-013-0399-0
17. Giles, M.B., Pierce, N.A.: An introduction to the adjoint approach to design. Flow Turbul. Combust. **65**(3–4), 393–415 (2000)
18. Jameson, A., Martinelli, L.: Aerodynamic Shape Optimization Techniques Based on Control Theory. Springer, Berlin (2000)
19. Raffard, R.L., Amonlirdviman, K., Axelrod, J.D., Tomlin, C.J.: An adjoint-based parameter identification algorithm applied to planar cell polarity signaling. IEEE Trans. Autom. Control **53**(Special Issue), 109–121 (2008)
20. Bressan, A., Guerra, G.: Shift-differentiability of the flow generated by a conservation law. Discrete Contin. Dyn. Syst. **3**(1), 35–58 (1997)
21. Ulbrich, S.: A sensitivity and adjoint calculus for discontinuous solutions of hyperbolic conservation laws with source terms. SIAM J. Control Optim. **41**(3), 740–797 (2002)
22. Ulbrich, S.: Adjoint-based derivative computations for the optimal control of discontinuous solutions of hyperbolic conservation laws. Syst. Control Lett. **48**(3), 313–328 (2003)
23. Jacquet, D., de Wit, C.C., Koenig, D.: Optimal ramp metering strategy with extended LWR model; analysis and computational methods. In: Proceedings of the 16th IFAC World Congress (2005)
24. Moin, P., Bewley, T.: Feedback control of turbulence. Appl. Mech. Rev. **47**(6S), S3 (1994)
25. Reuther, J., Jameson, A., Farmer, J., Martinelli, L., Saunders, D.: Aerodynamic Shape Optimization of Complex Aircraft Configurations via an Adjoint Formulation. Research Institute for Advanced Computer Science, NASA Ames Research Center, Mountain View (1996)

26. Müller, J.D., Cusdin, P.: On the performance of discrete adjoint CFD codes using automatic differentiation. Int. J. Numer. Methods Fluids **47**(8–9), 939–945 (2005)
27. Giering, R., Kaminski, T.: Recipes for adjoint code construction. ACM Trans. Math. Softw. **24**(4), 437–474 (1998)
28. Giles, M.B.: Discrete adjoint approximations with shocks. In: Hyperbolic Problems: Theory, Numerics, Applications, pp. 185–194. Springer, Berlin (2003)
29. Giles, M., Ulbrich, S.: Convergence of linearized and adjoint approximations for discontinuous solutions of conservation laws. Part 2: Adjoint approximations and extensions. SIAM J. Numer. Anal. **48**(3), 905–921 (2010)
30. Banda, M.K., Herty, M.: Adjoint imex-based schemes for control problems governed by hyperbolic conservation laws. Comput. Optim. Appl. **51**(2), 909–930 (2012)
31. Nessyahu, H., Tadmor, E.: Non-oscillatory central differencing for hyperbolic conservation laws. J. Comput. Phys. **87**(2), 408–463 (1990)
32. Strub, I.S., Bayen, A.M.: Weak formulation of boundary conditions for scalar conservation laws: an application to highway traffic modelling. Int. J. Robust Nonlinear Control **16**(16), 733–748 (2006)
33. Giles, M., Pierce, N.: Adjoint equations in CFD: duality, boundary conditions and solution behaviour. AIAA Pap. **97**(1850), 182–198 (1997)
34. Castaings, W., Dartus, D., Honnorat, M., Le Dimet, F.-X., Loukili, Y. Monnier, J.: Automatic differentiation: a tool for variational data assimilation and adjoint sensitivity analysis for flood modeling. In: Automatic Differentiation: Applications, Theory, and Implementations, vol. 50, pp. 249–262. Springer, Berlin (2006)
35. Jacquet, D., de Wit, C., Koenig, D.: Traffic control and monitoring with a macroscopic model in the presence of strong congestion waves. In: 44th IEEE Conference on Decision and Control, pp. 2164–2169. IEEE (2005)
36. Gomes, G., Horowitz, R.: Optimal freeway ramp metering using the asymmetric cell transmission model. Transp. Res. C Emerg. Technol. **14**(4), 244–262 (2006)
37. Ziliaskopoulos, A.K.: A linear programming model for the single destination system optimum dynamic traffic assignment problem. Transp. Sci. **34**(1), 37 (2000)
38. Muralidharan, A., Horowitz, R.: Optimal control of freeway networks based on the link node cell transmission model. In: American Control Conference (ACC), pp. 5769–5774. IEEE (2012)
39. Fugenschuh, A., Herty, M., Klar, A., Martin, A.: Combinatorial and continuous models for the optimization of traffic flows on networks. SIAM J. Optim. **16**(4), 1155–1176 (2006)
40. D'Apice, C., Gottlich, S., Herty, M., Piccoli, B.: Modeling, Simulation, and Optimization of Supply Chains: A Continuous Approach. SIAM, Philadelphia (2010)
41. Ramón, J., Frejo, J., Camacho, E.F.: Global versus local MPC algorithms in freeway traffic control with ramp metering and variable speed limits. IEEE Trans. Intell. Transp. Syst. **13**(4), 1556–1565 (2013)
42. Ben-Akiva, M., Cuneo, D., Hasan, M.: Evaluation of freeway control using a microscopic simulation laboratory. Transp. Res. C Emerg. Technol. **11**(1), 29–50 (2003)
43. Richards, P.: Shock waves on the highway. Oper. Res. **4**(1), 42–51 (1956)
44. Lighthill, M., Whitham, G.: On kinematic waves. II. A theory of traffic flow on long crowded roads. Proc. R. Soc. Lond. Ser. A Math. Phys. Sci. **229**(1178), 317 (1955)
45. Daganzo, C.F.: The cell transmission model. Part II: Network traffic. Transp. Res. B Methodol. **29**(2), 79–93 (1995)
46. Papageorgiou, M., Hadj-Salem, H., Blosseville, J.: Alinea: a local feedback control law for on-ramp metering. Transp. Res. Rec. **1320**, 58–64 (1991)
47. Papamichail, I., Papageorgiou, M., Vong, V., Gaffney, J.: Heuristic ramp-metering coordination strategy implemented at monash freeway, australia. Transp. Res. Rec. J. Transp. Res. Board **2178**(1), 10–20 (2010)
48. Kachroo, P.: Feedback Ramp Metering in Intelligent Transportation Systems. Springer, Berlin (2003)
49. Chen, O., Hotz, A., Ben-Akiva, M.: Development and evaluation of a dynamic ramp metering control model. Technical report (1997)
50. Bressan, A.: Hyperbolic Systems of Conservation Laws, Oxford Lecture Series in Mathematics and Its Applications, vol. 20. Oxford University Press, Oxford (2000)
51. Evans, L.C.: Partial Differential Equations. Graduate Studies in Mathematics. American Mathematical Society, Providence (1998)
52. Godunov, S.K.: A difference method for numerical calculation of discontinuous solutions of the equations of hydrodynamics. Matematicheskii Sbornik **89**(3), 271–306 (1959)

53. Wächter, A., Biegler, L.T.: On the implementation of an interior-point filter line-search algorithm for large-scale nonlinear programming. Math. Program. **106**(1), 25–57 (2006)
54. Flasskamp, K., Murphey, T., Ober-Blobaum, S.: Switching time optimization in discretized hybrid dynamical systems. In: IEEE 51st Annual Conference on Decision and Control (CDC), pp. 707–712. IEEE (2012)
55. Delle Monache, M.L., Reilly, J., Samaranayake, S., Krichene, W., Goatin, P., Bayen, A.M.: A PDE–ODE model for a junction with ramp buffer. SIAM J. Appl. Math. **74**(1), 22–39 (2014)
56. Fiacco, A.V., McCormick, G.P.: Nonlinear Programming: Sequential Unconstrained Minimization Techniques, vol. 4. SIAM, Philadelphia (1990)
57. Boyd, S., Vandenberghe, L.: Convex Optimization, vol. 25. Cambridge University Press, Cambridge (2010)
58. Chen, C., Petty, K., Skabardonis, A., Varaiya, P., Jia, Z.: Freeway performance measurement system: mining loop detector data. Transp. Res. Rec. J. Transp. Res. Board **1748**(1), 96–102 (2001)
59. Skabardonis, A., Varaiya, P., Petty, K.: Measuring recurrent and nonrecurrent traffic congestion. Transp. Res. Rec. **1856**(03), 118–124 (2003)